Newton

Article

Heterogeneous dynamics in a polymer solution revealed through measurement of ultraslow convection

Graphical abstract

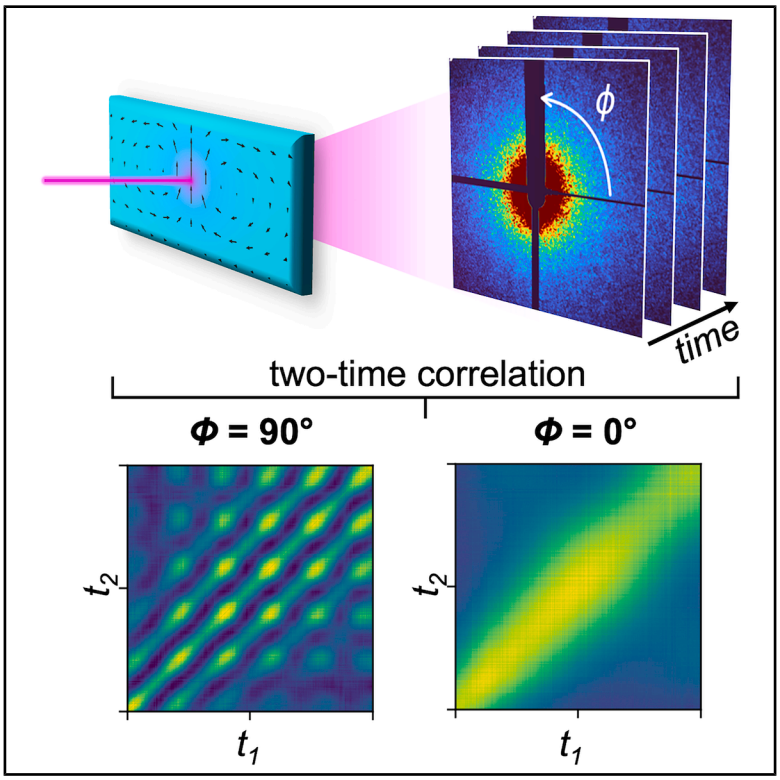

Highlights

- X-ray photon correlation spectroscopy reveals ultraslow convection
- Ångstrom-per-second flow measured directly in a polymer solution
- Beam-induced heating alters dynamics without changing structure
- Mobile polymer clusters and tangled networks coexist in solution

Authors

Thomas P. Chaney, Samuel D. Marks, Dylan M. Ladd, ..., Amnahir E. Peña-Alcántara, Hans-Georg Steinrück, Michael F. Toney

Correspondence

h.steinrueck@fz-juelich.de (H.-G.S.), michael.toney@colorado.edu (M.F.T.)

In brief

Ultraslow dynamics are key to understanding relaxation and aging in soft-matter systems and yet can be challenging to measure. Chaney et al. use X-ray photon correlation spectroscopy to uncover ultraslow convection and hidden structural complexity in a polymer solution, showing that modest beam heating alters material dynamics without changing structure, highlighting an important consideration for interpreting X-ray measurements of time-dependent behavior.

Chaney et al., 2026, Newton *2*, 100464
July 6, 2026
https://doi.org/10.1016/j.newton.2026.100464

CellPress

Newton

CellPress
OPEN ACCESS

Article

Heterogeneous dynamics in a polymer solution revealed through measurement of ultraslow convection

Thomas P. Chaney,[1] Samuel D. Marks,[1] Dylan M. Ladd,[1] Andrei Fluerasu,[2] Federico Zontone,[3] Yuriy Chushkin,[3] Sebastian Früchtl,[4,5] Dina Sheyfer,[6] Kelsey Levine,[1] Amnahir E. Peña-Alcántara,[8] Hans-Georg Steinrück,[4,5,7,*] and Michael F. Toney[1,9,10,*]

[1]Materials Science and Engineering, University of Colorado, Boulder, CO 80309, USA
[2]National Synchrotron Light Source II, Brookhaven National Laboratory, Upton, NY 11973-5000, USA
[3]ESRF - The European Synchrotron, 71 Avenue des Martyrs, CS 40220, 38043 Grenoble Cedex, France
[4]Institute for a sustainable Hydrogen Economy (IHE-1), Forschungszentrum Jülich, An der Deutschen Welle 7a, 52428 Jülich, Germany
[5]Institute of Physical Chemistry, RWTH Aachen University, Landoltweg 2, 52074 Aachen, Germany
[6]X-ray Science Division, Argonne National Laboratory, Argonne, IL 60439, USA
[7]Department of Chemistry, Paderborn University, Warburger Straße 100, 33098 Paderborn, Germany
[8]Department of Materials Science and Engineering, Stanford University, Stanford, CA 94305, USA
[9]Department of Chemical and Biological Engineering and Renewable and Sustainable Energy Institute (RASEI), University of Colorado, Boulder, CO 80309, USA
[10]Lead contact
*Correspondence: h.steinrueck@fz-juelich.de (H.-G.S.), michael.toney@colorado.edu (M.F.T.)
https://doi.org/10.1016/j.newton.2026.100464

ACCESSIBLE OVERVIEW Controlling how molecules move and organize within liquids is important for the development and improvement of many modern technologies, from solar energy materials to coatings and advanced plastics. However, these motions can be extremely slow and difficult to observe and quantify, especially in complex polymer solutions where standard optical techniques often fail. In this study, we used a sensitive X-ray method to directly measure how clusters of polymers move in solution. We discovered that even small amounts of heat from the X-ray beam can create tiny upward currents in the liquid, causing material to drift at extremely slow speeds. These subtle flows revealed that the solution contains a mixture of freely moving clusters and more tangled, network-like structures. Understanding this hidden organization is important because molecular assembly in solution often determines the structure and performance of a final solid material coated from the solution, including those used in organic solar cells and printed electronic devices. More broadly, our results show that measurement tools themselves can influence the behavior of soft matter, even when no obvious structural changes are visible. Recognizing and accounting for these effects will help researchers make more accurate measurements of slow dynamics in liquids. At the same time, the ability to detect such gentle motion opens new opportunities to study how complex fluids evolve, relax, and respond to their environment, improving our understanding of materials that play key roles in energy, manufacturing, and emerging technologies.

SUMMARY

Understanding solution-phase aggregation and dynamics in complex fluids is critical for material processing, yet widely used dynamic light scattering (DLS) is unsuitable for strongly attenuating systems such as conjugated polymers. We use X-ray photon correlation spectroscopy (XPCS) to probe the dynamics of a polymer, PM7, in toluene, revealing unexpected oscillations in the autocorrelation function that show vertical flow during measurement. Despite the relatively low X-ray absorption, measured flow velocities scale with X-ray power and suggest convective transport. Our analyses reveal mobile and static scatterers that together produce oscillatory, heterodyne features in the correlation functions. Finite element simulations predict flow velocities much larger than observed, suggesting that entanglements of the aggregates slow their motion. These results provide a direct measurement of ultraslow convection and highlight the need to account for

even modest beam heating in XPCS analysis. Moreover, the observation of distinct scatterer populations underscores the structural complexity of conjugated polymer solutions.

INTRODUCTION

Particle size and motion in liquid-phase suspensions are of great importance toward understanding materials processing and function across a variety of fields, including pharmaceuticals, polymers, and nanoparticles. Particularly, dynamics in the ultraslow regime of Å/s motion are key to understanding stress relaxation, gel formation, and aging in soft-matter systems. Dynamic light scattering (DLS) is one tool that is commonly used to probe the size and dynamics of nanoparticles, polymer aggregates, and proteins in solution. DLS measures dynamics through the decay of the scattering-vector ($\vec{q}$)-dependent time autocorrelation function of speckle intensities due to nanoscale dynamics. Additionally, measurements of various flow fields have been demonstrated through oscillations of the autocorrelation function.[1,2] A limitation of DLS is its non-applicability to solutions/particles that strongly absorb light and exhibit multiple scattering effects at the probing wavelength. These effects may reduce the scattered signal strength and introduce unintended dynamics.[3] Unintended dynamics may arise from convective flows caused by local heating of the solution due to light absorption. Convective flow has been observed using DLS in numerous materials, including conjugated polymers, hemoglobin, and gold nanoparticles.[4–9] The flow has also been imaged using tracer particles to visualize the convective cycles.[10] Quantification of these convective flows has remained elusive due to the inability of most DLS experiments to accurately probe scattering with vertical $\vec{q}$ components.[5] Therefore, the nature of light-absorption-induced convective currents and strategies to mitigate them remain poorly understood.

X-ray photon correlation spectroscopy (XPCS) presents new opportunities to better characterize ultraslow dynamics by using area detectors that simultaneously record scattering in both vertical and horizontal $\vec{q}$ directions, spanning several decades in q.[11–16] Also, X-rays have lower attenuation in most materials compared to visible light. Thus, XPCS can potentially overcome the limitations of DLS in measuring optically opaque solutions. In XPCS and DLS, the velocity of scatterers within a sample can be probed in homodyne or heterodyne modality.[16–18] Homodyne experiments probe the relative difference in velocity between scatterers, while heterodyne experiments resolve velocities through the use of a static reference scatterer.[14,16]

In this study, we use XPCS to probe the dynamics of aggregate structures present in a solution of a state-of-the-art conjugated polymer, poly[(2,6-(4,8-bis(5-(2-ethylhexyl)-4-chlorothiophen-2-yl)-benzo[1,2-b:4,5-b']dithiophene))-alt-(5,5-(1′,3′-di-2-thienyl)-5′,7′-bis(2-ethylhexyl)benzo[1′,2′-c:4′,5′-c']dithiophene-4,8-dione))], referred to as PM7, in toluene. The chemical structure of PM7 is shown in Figure S1. PM7 and similar polymers have achieved high performance in organic photovoltaic devices, particularly by tuning solution aggregation using methods including shearing forces.[19–21] Yet, the understanding of the nature of solution aggregates in these polymer solutions remains incomplete, motivating the study of this system with XPCS. By performing XPCS experiments with varying X-ray beam power and small- vs. large-beam sizes (see methods), we identify unexpected oscillations in the autocorrelation functions that indicate vertical convective flow driven by local beam heating despite the relatively low attenuation of X-rays in the sample. Our analyses of these autocorrelation functions reveal the presence of both mobile and quasi-static polymer aggregates, producing internal heterodyne mixing. Furthermore, the slower-than-expected flow velocities suggest that the mobile polymer aggregates are likely constrained by entanglements, leading to non-Newtonian flow behavior. Our results underscore the complex, entangled aggregate structures in solution-processed conjugated polymers and highlight the need to account for beam-induced heating in XPCS experiments on liquid samples.

RESULTS

XPCS and small-angle scattering analysis

Single detector frames exhibiting speckle patterns are shown for measurements taken at small-beam and large-beam conditions in Figures 1A and 1D, respectively. The two-time correlation functions (TTCFs) for PM7 in toluene are plotted in Figures 1B and 1C for small-beam conditions with 47% of an unattenuated beam flux at q = 0.005 Å^{-1} at $\phi = 90^\circ$ and $\phi = 0^\circ$. Oscillations appear at $\phi = 90^\circ$ (Figure 1B) along both the constant-lag and the constant-age directions. These directions are shown in Figure 1F, and their definition and meaning are described in detail elsewhere.[22,23] The checkerboard pattern in Figure 1B has been previously observed in epitaxial growth experiments[24,25] and for shear-thickening colloids.[26] All oscillations disappear at $\phi = 0^\circ$ (Figure 1C), indicating that they are caused by anisotropic dynamics such as directional flow.[12,15] The ϕ dependence of the TTCF features is apparent at a range of q values and across all measurements, as shown in Figures S2, S3, and S4.

Importantly, the time-dependent small-angle X-ray scattering (SAXS) data shown in Figure S5 show no significant changes in scattering across the measurement time that would suggest beam-induced structural evolution. This observation casts significant doubt on the validity of the typical approach of using a constant scattering intensity (i.e., constant $S(q)$) as a proxy for the maximum dose at which intrinsic sample dynamics are still measurable (i.e., non-beam-altered $S(q, \omega)$).[27] While noting that each sample system may behave differently with regard to "beam damage," our results unambiguously show that a constant static $S(q)$ is not a proxy, or even an approximation thereof, for a constant dynamic $S(q, \omega)$ (even for cases when this changes along the lag time [Figures S2, S3, and S4]). In this context, Figures S6 and S7 confirm isotropy in the scattering pattern and consistency of the azimuthally integrated $I(q)$ between measurements, respectively.

To understand the oscillations in correlation intensity along the constant-lag direction (Figure 1B), we analyze the large-beam data shown in Figures 1E and 1F. The TTCF shows no

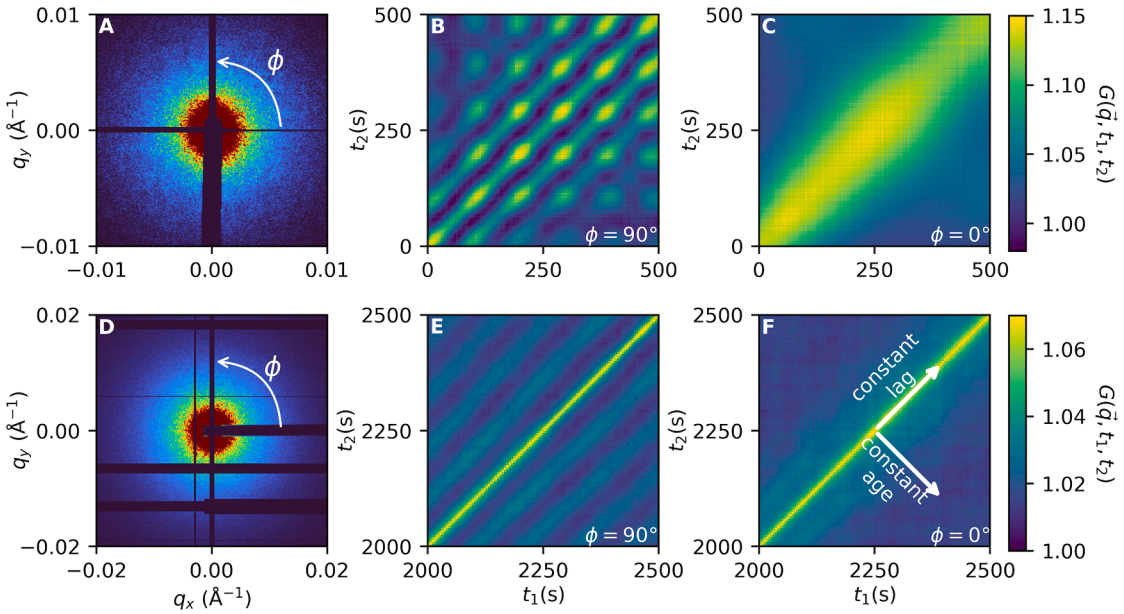

Figure 1. Detector frames from small- and large-beam experiments and calculated TTCFs

(A) Linearly scaled detector frame from small-beam scattering at 47% beam flux with 0.5 s readout time.

(B) TTCF of small-beam data taken at q = 0.0045–0.0055 Å^{-1} and $\phi = 90°$.

(C) TTCF of small-beam data taken at q = 0.0045–0.0055 Å^{-1} and $\phi = 0°$.

(D) Linearly scaled detector frame from large-beam scattering at 100% beam flux with a 5 s readout time.

(E) TTCF of large-beam data taken at q = 0.0185 Å^{-1} and $\phi = 90°$.

(F) TTCF of large-beam data taken at q = 0.0185 Å^{-1} and $\phi = 0°$.

Note that only a middle portion of the TTCF is shown in (E) and (F) to allow for easy comparison with (B) and (C), as well as to avoid bad frames. Full TTCFs are shown in Figures S2, S3, and S4.

oscillations along the constant-lag direction but still exhibits a similar oscillation trend along the constant-age diagonal with varying ϕ, compared to the small-beam data. Given the ~40× greater beam area in the large-beam experiments, we suggest that the oscillations along the constant-lag direction seen in the small-beam data (Figure 1B) are likely due to the X-ray probe capturing local dynamics that produce periodically increased speckle contrast, which averages out with a larger beam cross-section. Indeed, waterfall plots in Figure S8 show concurrent speckle appearance and disappearance in the small-beam data that account for the changes in contrast. The small-beam cross-section captures the local motion of a single or a small number of aggregates, which would produce concurrent, cyclical fluctuations of speckles from the heterodyne contrast described below. We can roughly estimate the number of aggregates within the beam volume using the polymer volume fraction of ~1% in the solution. Using an estimated cylindrical aggregate diameter of 100 Å from previous studies[28] and a length of 1,500 Å, corresponding to the average molecular weight of the PM7, we estimate ~23 million aggregates within the small-beam volume. However, previous SAXS studies suggest significant polydispersity in aggregate size,[28] and our XPCS is only probing q ranges corresponding to aggregate diameters >500 Å. Additionally, each slice of the X-ray detector only encompasses a small portion of the orientation sphere for our isotropic liquid sample. For these reasons, it is plausible that only a relatively small number of individual aggregates are producing speckles captured in the small-beam TTCFs. A similar strategy employing a focused beam was recently used to reveal similar local motion of scatterers through heterodyne behavior in shear-thickening colloidal solutions.[26]

Modeling the XPCS autocorrelation function

To gain further insight into the origin of the heterodyne-like oscillations in the TTCFs, we model the g_2 autocorrelation functions, obtained by time averaging the TTCF along the constant-lag direction, as shown in Figure 1F.[22,23] The g_2 functions averaged over the middle 50 s of the total scan time across a range of azimuthal angles are plotted in Figure 2. The oscillation frequency in the g_2 functions depends on the q bin, as shown in Figure S9, consistent with previous XPCS experiments on systems with flow.[16,26] We first attempted to use a homodyne model, which was unable to fit the data (Figure S10).[13] Instead, we found that the experimental g_2 functions are modeled well by a heterodyne system characterized by mobile and static scattering populations represented by Equation 1.[29,30]

$$g_2(\vec{q},\tau) = 1 + \beta\Big(X^2\left|g_{1,A}(\vec{q},\tau)\right|^2 + (1-X)^2\left|g_{1,B}(\vec{q},\tau)\right|^2 + 2X(1-X)Re\Big[g_{1,A}(\vec{q},\tau)\cdot g^*_{1,B}(\vec{q},\tau)\Big]\Big) \quad \text{(Equation 1)}$$

In Equation 1, β is the contrast, X is the fraction of scattering from the mobile scatterers, and $g_{1,A}$ and $g_{1,B}$ correspond to the

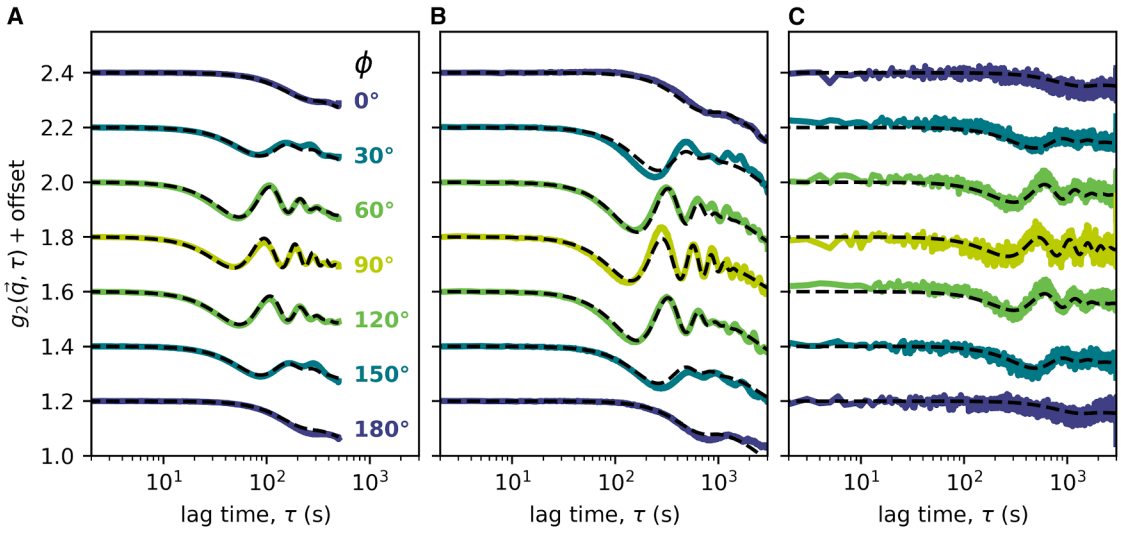

Figure 2. Autocorrelation functions and fits

Autocorrelation (g_2) functions (solid lines) and fits (dashed lines) for small-beam data obtained using an average over the middle 50 s of the total scan time of the TTCFs. Cuts shown are obtained from TTCFs evaluated at various ϕ values with a width of 30° and a q range of 0.0045–0.0055 Å^{-1}. Fits for three beam intensities are shown with (A) 47%, (B) 9%, and (C) 1% of unattenuated flux. Curves are vertically offset by 0.2 for clarity.

intermediate scattering functions of mobile and quasi-static scatterers, respectively, given by Equations 2 and 3.

$$g_{1,A}(\vec{q},\tau) = e^{-\left(\frac{|\vec{v}|^2\tau^2}{4\sigma^2}\right)} e^{i\tau\vec{q}\cdot\vec{v}} e^{-(\Gamma_A\tau)^{\alpha_A}} \quad \text{(Equation 2)}$$

$$g_{1,B}(\vec{q},\tau) = e^{-(\Gamma_B\tau)^{\alpha_B}} \quad \text{(Equation 3)}$$

In Equation 2, there are two terms related to the drift velocity of the particles: first, a beam transit term to describe decorrelation of particles transiting out of a Gaussian-shaped beam with a root-mean-squared width σ, and second, an oscillatory term that produces the characteristic heterodyne ripples. Oscillations only appear in the TTCFs extracted from scattering bins that contain a vertical component of q, showing that the direction of the flow is vertical. Values of $|\vec{v}|$ from the fits shown in Figure 2 indicate flow with velocities ranging from 3 to 13 Å/s, depending on X-ray beam flux. Complete fit parameters are available in Tables S1, S2, S3, and S4. We note that this model is likely a simplification of the actual system, which has a range of Γ_A, Γ_B, α_A, and α_B reflecting the polydispersity in aggregate size common for conjugated polymers like PM7.[28,31] Additionally, the heterodyne terms dominate the model, resulting in large uncertainties of relaxation rates and stretching exponents. This is even true for the experimental g_2 functions taken at horizontal directions, as the slice width of 30° means the heterodyne component accounts for ~50% of the decrease in the g_2 value at the bottom of the first shoulder seen in ϕ = 0° and 180° curves (Figure 2) based on our fit parameters. We expect that future experiments with more monodisperse particle characteristics and optimized detector geometry will be able to extract reliable characteristic decorrelation rates and stretching exponents from analysis of XPCS collected at scattering vectors perpendicular to the flow.

Nonetheless, the strong heterodyne oscillations allow reliable extraction of velocities and indicate that there are two populations of scatterers–one mobile and one quasi-static. These two populations can be explained through the presence of both mobile polymer aggregates and a static polymer network of aggregates. Previous SAXS and cryoelectron microscopy (cryo-EM) studies of PM7 in chlorobenzene solutions support this explanation, suggesting the presence of a complex population of aggregates exhibiting both isolated and networked structures.[28,31] It is worth pointing out that equivalent g_2 functions may also be produced by using two mobile scattering populations with a constant offset in drift velocity. However, this scenario is unlikely given the broad polydispersity inherent in PM7 solution aggregates.[28,31]

Modeling vertical aggregate motion

Having established the origin of the internal heterodyne mixing, we now discuss the driving force for the vertical motion of the mobile aggregates. In the XPCS experiment, the horizontally mounted capillary was sealed on both ends, and no external fields were applied. Thus, the vertical motion must be due to gravity—the only force acting on the aggregates in the vertical direction. Gravity can drive vertical flow of aggregates through sedimentation or buoyancy due to a density difference relative to the surrounding matrix.

To understand whether sedimentation or buoyancy is driving the vertical velocity, we examine the dependence of fitted velocity on X-ray beam flux. The vertical velocities extracted from the fits in Figure 2 are plotted vs. the absorbed X-ray power density in Figure 3, revealing a linear dependence. While X-ray absorption can have many effects on a sample, the lack of major structural rearrangements, indicated by the unchanged SAXS profile and intensity and the identification of gravity as the driving force, suggest that local heating due to X-ray absorption is the main factor.

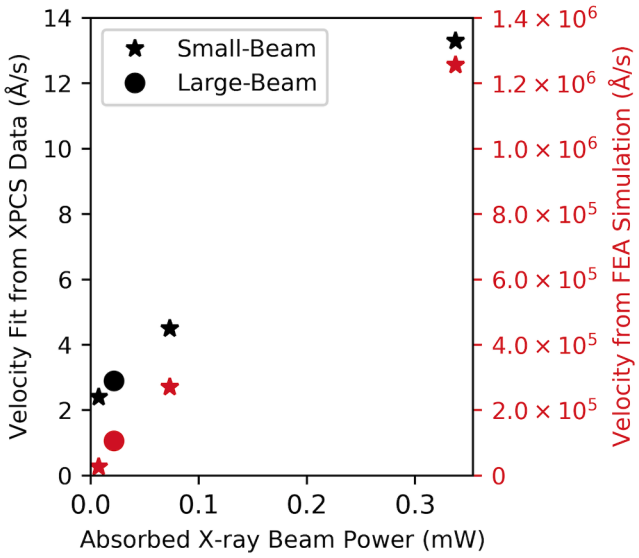

Figure 3. XPCS-fitted and FEA-predicted velocities

Comparison of velocities from XPCS analysis (black markers, left axis) and FEA simulation (red markers, right axis) plotted against X-ray beam power. Stars correspond to data from small-beam footprints, while filled circles correspond to large-beam footprints.

Local heating of a fluid decreases the dynamic viscosity, η, and solvent density, $\rho_{solvent}$, while the particle density, $\rho_{particle}$, remains the same. Therefore, the sedimentation speed, v, will increase under the acceleration of gravity, g, as approximated through the Stokes equation:

$$v = \frac{2gr^2\left(\rho_{particle} - \rho_{solvent}\right)}{9\eta}. \quad \text{(Equation 4)}$$

However, using an approximate aggregate radius, r, of 100 Å found in previous solution SAXS studies[28] and the tabulated temperature-dependent viscosity and density of toluene, we find that the temperature of the solution within the beam volume would need to reach ~210°C for sedimentation to explain the velocities, an unrealistic temperature higher than the boiling point of toluene (Figure S11).

We are now left with convective currents driven by the buoyant locally heated solvent dragging aggregates upward as the only reasonable mechanism driving the vertical velocity. Indeed, this effect has been identified as a driving force for beam-induced vertical flow in DLS experiments.[4–8] However, most DLS experiments are unable to accurately measure velocities due to uncertainty in the vertical scattering vector caused by thermal lensing.[5] Our XPCS measurements present the opportunity to directly compare velocities fitted from autocorrelation functions to predicted velocities via fluid dynamics models.

To find the fluid velocities that can be expected from beam-induced convection, we perform finite element analysis (FEA) of a two-dimensional (2D) representation of our experiment using COMSOL Multiphysics software. The X-ray beam absorption is modeled as a 2D Gaussian heat source, and the capillary walls are held at a temperature of 20°C. In our FEA simulations, we utilize the material properties of neat toluene, since viscosity measurements of the PM7 solution, as shown in Figure S12, indicate little deviation from the behavior of pure toluene. Full details of the FEA simulations are included in the supplemental information (see Note S1 and Table S5), and an example of the flow field and temperature distribution from a steady-state solution for the XPCS experiment is shown in Figures S13 and S14. We compare the vertical velocity in the beam volume from the simulations with results from XPCS analysis in Figure 3. While the velocities predicted from FEA also increase monotonically with beam power, they are surprisingly several orders of magnitude faster than velocities obtained from XPCS autocorrelation function fits. Our data exhibiting correlations in the g_2 that persistent for hundreds of seconds (Figure 2) clearly show that the scatterers are not moving at ~1 μm/s velocities as predicted by the FEA analysis, since the decorrelation time due to transit of scatterers outside of the beam height (4.6 μm full width at half maximum) would be on the order of 1–10 s for such velocities.

One explanation may be the competing sedimentation velocity of these particles in the opposite direction. However, as shown in Figure S11, we expect the sedimentation velocity for ~100 Å aggregates to be on the order of Å/s, not nearly enough to impact the vertical convective flows of μm/s estimated from FEA simulations. It is also possible that the previously assumed static population of aggregates is also mobile. However, it is also unlikely that we have a purely bimodal distribution of aggregate velocities giving rise to strong heterodyne features. Instead, we propose that the viscosity of the solution at these very low shear rates is much larger than the viscosity of pure toluene. Our viscosity measurements in Figure S12 were taken at a shear rate of ~20,000 s^{-1}, several orders of magnitude higher than the estimated shear in the solution of <1 s^{-1}. Polymer solutions are known to exhibit a non-Newtonian shear-thinning behavior, where at very low shear rates a solution may have orders-of-magnitude greater viscosities caused by weak entanglements that provide resistance to flow at low shears but that are easily broken at higher shears.[32] A study of a similar conjugated polymer in solution with chlorobenzene found that dilute solutions exhibit low-shear rate viscosities of over 10 Pa•s, four orders of magnitude larger than the viscosity of the neat solvent.[33] Using a value of 10 Pa•s for the viscosity produces flow rates on the order of 10 Å/s, in agreement with the XPCS data. We suggest that the drastic non-Newtonian behavior of conjugated polymer solution is responsible for the observed ultraslow convective velocities.

DISCUSSION

In this work, analysis of beam-induced flow has been used to reveal complex solution aggregate structures and dynamics for PM7, a high-performance conjugated polymer used in organic photovoltaics, while also underscoring key considerations in designing XPCS experiments for any (liquid) sample. By using X-rays instead of visible light, we circumvent the limitations imposed by strong attenuation and multiple scattering. However, we still found that the local heating from X-ray beam absorption produces convective currents with a velocity proportional to beam power. This phenomenon has been previously observed but not well quantified in DLS experiments. By

analyzing the autocorrelation function obtained at various azimuthal angles on the area detector, we reveal isolated vertical flow with velocities on the order of Å/s, a regime that has been inaccessible for DLS. These velocities are orders of magnitude slower than predicted by simple FEA simulations. We attribute the discrepancy in velocity to entangled aggregate structures that introduce shear-thinning behavior, resulting in viscosities at low shear rates of ~10 Pa•s.

Overall, this study underscores the complexity of aggregate structures within the solution for the PM7 polymer. Understanding the nature of these structures is vital to revealing the key to the high performance of PM7 and similar polymers in deposited films for organic photovoltaics. More broadly, we demonstrate that a constant scattering intensity profile (e.g., constant $S(q)$) is not sufficient to assume unchanging sample dynamics or the lack of beam-driven effects within the sample. Notably, we characterize X-ray-induced convection that is likely present in many solution-phase X-ray scattering and light scattering experiments—an effect that must be carefully considered for the design of future solution-phase XPCS and DLS experiments.

METHODS

Speckle patterns in the SAXS regime were collected from solutions of PM7 polymer in toluene solvent at the beamlines ID10-COH at ESRF and 11-ID at NSLS-II. PM7 was obtained from 1-Material, with a molecular weight of 120 kDa and a polydispersity index of 2.5. In both experiments, the solution was prepared by dissolving 10 mg of PM7 per mL of toluene and stirring for at least 3 h. These solutions were then transferred into a 1-mm-diameter quartz capillary with 10 μm wall thickness, sealed, and mounted horizontally in a metal sample cell at ambient temperature (~20°C). At ESRF ID10-COH, a small beam size of 40 μm^2 was used to produce an unattenuated flux density of 6.2×10^{10} photons/s/μm^2. Measurements were taken with three systematically varied upstream attenuators to achieve 47%, 9%, and 1% transmission of the unattenuated flux incident on the PM7 polymer solution with detector image collection times of 0.5, 0.5, and 1.0 s, respectively. To rule out any contribution by the experimental setup and further investigate the flux-density dependence, experiments were repeated at NSLS-II 11-ID with a much larger beam size of 1,600 μm^2, producing an unattenuated flux density of 6.3×10^7 photons/s/μm^2. Due to the lower flux density, detector images were collected at 5 s increments. We refer to the two experimental setups as small-beam and large-beam for the ESRF ID10 and NSLS-II 11-ID experiments, respectively. Additional details on the experimental setup are in Tables S6 and S7. For both experimental setups, we ensured that the longitudinal coherence condition is met for our maximum q value of 0.0185 $Å^{-1}$ (see Note S2; Figure S15, and Table S8). Data were analyzed using the beamlines' specific software.[34] For each set of detector images, we computed TTCFs spanning regions of the detector defined by a q range and azimuthal angle, ϕ.[22,23]

RESOURCE AVAILABILITY

Lead contact

Requests for further information and resources should be directed to and will be fulfilled by the lead contact, Michael F. Toney (michael.toney@colorado.edu).

Materials availability

This study did not generate new unique materials.

Data and code availability

- XPCS detector images, TTCFs, COMSOL files, and Python code for analysis of TTCFs have been deposited at Zenodo with the identifier https://doi.org/10.5281/zenodo.18237958 and are publicly available as of the date of publication.
- Any additional information required to reanalyze the data reported in this paper is available from the lead contact upon request.

ACKNOWLEDGMENTS

This work was supported by the Office of Naval Research MURI Program Center for Self-Assembled Organic Electronics (SOE), grant N00014-19-1-2453. T.P.C. acknowledges support from the National Science Foundation Graduate Research Fellowship Program (NSF-GRFP) under grant no. DGE 2040434. A portion of the XPCS characterization was conducted at beamline 11-ID of the National Synchrotron Light Source II, a US Department of Energy (DOE) Office of Science User Facility operated for the DOE Office of Science by Brookhaven National Laboratory under contract no. DE-SC0012704. We also acknowledge the European Synchrotron Radiation Facility (ESRF) for providing synchrotron radiation facilities for another portion of the XPCS characterization under proposal number MA-5746 using beamline ID10-COH. D.M.L. acknowledges support from the NSF Center for Integration of Modern Optoelectronic Materials on Demand (IMOD) under cooperative agreement no. DMR-2019444 and from the GRFP (NSF-GRFP) under grant no. DGE 2040434. H.-G.S. and S.F. acknowledge the funding by the German Federal Ministry of Research, Technology and Space (BMFTR) and the Ministry of Economic Affairs, Industry, Climate Action and Energy of the state of North Rhine-Westphalia through project HC-H2 and from the BMFTR via projects 05K22PP2 and 05K24CJ2. A.E.P.-A. acknowledges support from the NSF-GRFP under grant no. DGE 1656518, as well as the Stanford Knight-Hennessy Scholarship and the Stanford Enhancing Diversity in Graduate Education Doctoral Fellowship. We are grateful for Ankur Gupta's assistance and fruitful discussions on fluid dynamics calculations. D.S. acknowledges the U.S. DOE Office of Science-Basic Energy Sciences, under Contract No. DEAC02-06CH11357.

AUTHOR CONTRIBUTIONS

Conceptualization, T.P.C., S.D.M., D.M.L., and M.F.T.; formal analysis, T.P.C., Y.C., A.F., and F.Z.; investigation, T.P.C., S.D.M., D.M.L., A.F., F.Z., Y.C., S.F., D.S., K.L., A.E.P.-A., H.-G.S., and M.F.T.; writing—original draft, T.P.C.; writing—review & editing, T.P.C., S.D.M., D.M.L., A.F., F.Z., Y.C., S.F., D.S., K.L., A.E.P.-A., H.-G.S., and M.F.T.; funding acquisition, M.F.T. and H.-G.S.

DECLARATION OF INTERESTS

The authors declare no competing interests.

DECLARATION OF GENERATIVE AI AND AI-ASSISTED TECHNOLOGIES IN THE WRITING PROCESS

During the preparation of this work, the authors used ChatGPT to improve the grammar and flow of the text. After using this tool/service, the authors reviewed and edited the content as needed and take full responsibility for the content of the published article.

SUPPLEMENTAL INFORMATION

Supplemental information can be found online at https://doi.org/10.1016/j.newton.2026.100464.

Received: October 7, 2025
Revised: January 15, 2026
Accepted: February 27, 2026
Published: March 23, 2026

REFERENCES

1. Fuller, G.G., Rallison, J.M., Schmidt, R.L., and Leal, L.G. (1980). The measurement of velocity gradients in laminar flow by homodyne light-scattering spectroscopy. J. Fluid Mech. *100*, 555–575. https://doi.org/10.1017/S0022112080001280.
2. López-Molina, J., Moncho-Jordá, A., and Tirado-Miranda, M. (2024). Measuring Absolute Velocities from Nonequilibrium Oscillations via Single-Detector 3D Dynamic Light Scattering. Phys. Rev. Lett. *133*, 198202. https://doi.org/10.1103/PhysRevLett.133.198202.
3. Fischer, K., and Schmidt, M. (2016). Pitfalls and novel applications of particle sizing by dynamic light scattering. Biomaterials *98*, 79–91. https://doi.org/10.1016/j.biomaterials.2016.05.003.
4. Sehgal, A., and Seery, T.A.P. (1999). Anomalous Dynamic Light Scattering from Solutions of Light Absorbing Polymers. Macromolecules *32*, 7807–7814. https://doi.org/10.1021/ma9903106.
5. Moulin, E., Nyrkova, I.A., Giuseppone, N., Semenov, A.N., and Buhler, E. (2020). Homodyne dynamic light scattering in supramolecular polymer solutions: anomalous oscillations in intensity correlation function. Soft Matter *16*, 2971–2993. https://doi.org/10.1039/C9SM02480H.
6. Parashchuk, O.D., Laptinskaya, T.V., Ananieva, M.S., and Paraschuk, D.Y. (2011). Hyperdiffusive dynamics in conjugated polymer blends and fullerene absorbing solutions. Soft Matter *7*, 5585. https://doi.org/10.1039/c1sm05519d.
7. Hall, R.S., Oh, Y.S., and Johnson, C.S. (1980). Photon correlation spectroscopy in strongly absorbing and concentrated samples with applications to unliganded hemoglobin. J. Phys. Chem. *84*, 756–767. https://doi.org/10.1021/j100444a013.
8. Schaertl, W., and Roos, C. (1999). Convection and thermodiffusion of colloidal gold tracers by laser light scattering. Phys. Rev. E *60*, 2020–2028. https://doi.org/10.1103/PhysRevE.60.2020.
9. Ben-Yosef, N., Zweigenbaum, S., and Weitz, A. (1972). Mass motion as observed by light-beating spectroscopy. Appl. Phys. Lett. *21*, 436–437. https://doi.org/10.1063/1.1654446.
10. Boyd, R.D., and Vest, C.M. (1975). Onset of convection due to horizontal laser beams. Appl. Phys. Lett. *26*, 287–288. https://doi.org/10.1063/1.88148.
11. Galluzzo, M.D., Steinrück, H.-G., Takacs, C.J., Mistry, A., Grundy, L.S., Cao, C., Narayanan, S., Dufresne, E.M., Zhang, Q., Srinivasan, V., et al. (2024). Probing transference and field-induced polymer velocity in block copolymer electrolytes. Cell Rep. Phys. Sci. *5*, 101766. https://doi.org/10.1016/j.xcrp.2023.101766.
12. Möller, J., and Narayanan, T. (2017). Velocity Fluctuations in Sedimenting Brownian Particles. Phys. Rev. Lett. *118*, 198001. https://doi.org/10.1103/PhysRevLett.118.198001.
13. Busch, S., Jensen, T.H., Chushkin, Y., and Fluerasu, A. (2008). Dynamics in shear flow studied by X-ray Photon Correlation Spectroscopy. Eur. Phys. J. E *26*, 55–62. https://doi.org/10.1140/epje/i2007-10305-2.
14. Fluerasu, A., Kwasniewski, P., Caronna, C., Destremaut, F., Salmon, J.-B., and Madsen, A. (2010). Dynamics and rheology under continuous shear flow studied by x-ray photon correlation spectroscopy. New J. Phys. *12*, 035023. https://doi.org/10.1088/1367-2630/12/3/035023.
15. Steinrück, H.-G., Takacs, C.J., Kim, H.-K., Mackanic, D.G., Holladay, B., Cao, C., Narayanan, S., Dufresne, E.M., Chushkin, Y., Ruta, B., et al. (2020). Concentration and velocity profiles in a polymeric lithium-ion battery electrolyte. Energy Environ. Sci. *13*, 4312–4321. https://doi.org/10.1039/D0EE02193H.
16. Lhermitte, J.R.M., Rogers, M.C., Manet, S., and Sutton, M. (2017). Velocity measurement by coherent x-ray heterodyning. Rev. Sci. Instrum. *88*, 015112. https://doi.org/10.1063/1.4974099.
17. Livet, F., Bley, F., Ehrburger-Dolle, F., Morfin, I., Geissler, E., and Sutton, M. (2006). X-ray intensity fluctuation spectroscopy by heterodyne detection. J Synchrotron Rad *13*, 453–458. https://doi.org/10.1107/S0909049506030044.
18. Livet, F., Bley, F., Ehrburger-Dolle, F., Morfin, I., Geissler, E., and Sutton, M. (2007). Homodyne and heterodyne X-ray photon correlation spectroscopy: latex particles and elastomers. J. Appl. Crystallogr. *40*, s38–s42. https://doi.org/10.1107/S0021889807003561.
19. Yuan, J., Liu, D., Zhao, H., Lin, B., Zhou, X., Naveed, H.B., Zhao, C., Zhou, K., Tang, Z., Chen, F., and Ma, W. (2021). Patterned Blade Coating Strategy Enables the Enhanced Device Reproducibility and Optimized Morphology of Organic Solar Cells. Adv. Energy Mater. *11*, 2100098. https://doi.org/10.1002/aenm.202100098.
20. Giri, G., DeLongchamp, D.M., Reinspach, J., Fischer, D.A., Richter, L.J., Xu, J., Benight, S., Ayzner, A., He, M., Fang, L., et al. (2015). Effect of Solution Shearing Method on Packing and Disorder of Organic Semiconductor Polymers. Chem. Mater. *27*, 2350–2359. https://doi.org/10.1021/cm503780u.
21. Diao, Y., Zhou, Y., Kurosawa, T., Shaw, L., Wang, C., Park, S., Guo, Y., Reinspach, J.A., Gu, K., Gu, X., et al. (2015). Flow-enhanced solution printing of all-polymer solar cells. Nat. Commun. *6*, 7955. https://doi.org/10.1038/ncomms8955.
22. Bikondoa, O. (2017). On the use of two-time correlation functions for X-ray photon correlation spectroscopy data analysis. J. Appl. Crystallogr. *50*, 357–368. https://doi.org/10.1107/S1600576717000577.
23. Ragulskaya, A., Starostin, V., Zhang, F., Gutt, C., and Schreiber, F. (2024). On the analysis of two-time correlation functions: equilibrium versus non-equilibrium systems. J. Appl. Crystallogr. *57*, 1098–1106. https://doi.org/10.1107/S1600576724004618.
24. Zhang, X., Ulbrandt, J.G., Myint, P., Fluerasu, A., Wiegart, L., Zhang, Y., Nelson, C., Ludwig, K.F., and Headrick, R.L. (2024). Local step-flow dynamics in thin film growth with desorption. Phys. Rev. Materials *8*, 033403. https://doi.org/10.1103/PhysRevMaterials.8.033403.
25. Ju, G., Xu, D., Highland, M.J., Thompson, C., Zhou, H., Eastman, J.A., Fuoss, P.H., Zapol, P., Kim, H., and Stephenson, G.B. (2019). Coherent X-ray spectroscopy reveals the persistence of island arrangements during layer-by-layer growth. Nat. Phys. *15*, 589–594. https://doi.org/10.1038/s41567-019-0448-1.
26. Horwath, J.P., He, H., Lee, J., Jiang, Z., Chakraborty, S., Zhang, Q., Dufresne, E.M., Sutton, M., Sandy, A., Narayanan, S., and Lin, X.M. (2025). Heterogeneous Dynamics in Shear Thickening Colloids Revealed by Intrinsic Heterodyne Correlation Spectroscopy. Phys. Rev. Lett. *134*, 178202. https://doi.org/10.1103/PhysRevLett.134.178202.
27. Verwohlt, J., Reiser, M., Randolph, L., Matic, A., Medina, L.A., Madsen, A., Sprung, M., Zozulya, A., and Gutt, C. (2018). Low Dose X-Ray Speckle Visibility Spectroscopy Reveals Nanoscale Dynamics in Radiation Sensitive Ionic Liquids. Phys. Rev. Lett. *120*, 168001. https://doi.org/10.1103/PhysRevLett.120.168001.
28. Chaney, T.P., Mahajan, C.L., Ghasemi, M., Levin, A.J., White, K.P., Milner, S.T., Gomez, E.D., and Toney, M.F. (2025). Deciphering the Structure of PM6-Type Conjugated Polymer Aggregates in Solution and Film. Chem. Mater. *37*, 7882–7893. https://doi.org/10.1021/acs.chemmater.5c01540.
29. Lewis, R.M., Jackson, G.L., Maher, M.J., Kim, K., Lodge, T.P., Mahanthappa, M.K., Narayanan, S., and Bates, F.S. (2018). A new framework for X-ray photon correlation spectroscopy analysis from polycrystalline materials. Rev. Sci. Instrum. *89*, 123902. https://doi.org/10.1063/1.5051451.
30. Geissler, E. (2022). Dynamic Light Scattering in Gels and Solutions. Period. Polytech. - Chem. Eng. *66*, 525–535. https://doi.org/10.3311/PPch.19988.

31. Khasbaatar, A., Cheng, A., Jones, A.L., Kwok, J.J., Park, S.K., Komar, J.K., Lin, O., Jackson, N.E., Chen, Q., DeLongchamp, D.M., et al. (2023). Solution Aggregate Structures of Donor Polymers Determine the Morphology and Processing Resiliency of Non-Fullerene Organic Solar Cells. Chem. Mater. *35*, 2713–2729. https://doi.org/10.1021/acs.chemmater.2c02141.

32. Ryder, J.F., and Yeomans, J.M. (2006). Shear thinning in dilute polymer solutions. J. Chem. Phys. *125*, 194906. https://doi.org/10.1063/1.2387948.

33. Xie, B., Zhang, K., Hu, Z., Fang, H., Lin, B., Yin, Q., He, B., Dong, S., Ying, L., Ma, W., et al. (2020). Polymer Pre-Aggregation Enables Optimal Morphology and High Performance in All-Polymer Solar Cells. Sol. RRL *4*, 1900385. https://doi.org/10.1002/solr.201900385.

34. Paleo, P., Kieffer, J., and Chushkin, Y. (2021). Silx-Kit/dynamix: Dynamix v0.2: XPCS from PythonVersion v0.2 (Zenodo). https://doi.org/10.5281/ZENODO.5520626.